Engineering Structures 273 (2022) 115119

Contents lists available at ScienceDirect

Engineering Structures

journal homepage: www.elsevier.com/locate/engstruct

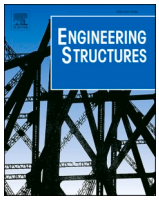

Effect of fatigue loading on flexural performance of NSM CFRP-strengthened RC beams under different service temperatures

Younes Jahani [a], Marta Baena [a,*], Cristina Barris [a], Lluís Torres [a], José Sena-Cruz [b]

[a] AMADE, Polytechnic School, University of Girona, 17003 Girona, Spain
[b] University of Minho, ISISE, Department of Civil Engineering, Guimarães, Portugal

ARTICLE INFO

Keywords:
Fatigue
NSM CFRP-strengthening
Temperature
Experimental

ABSTRACT

This paper presents an experimental work to investigate the effect of fatigue loading and high service temperature on the flexural performance of near-surface mounted (NSM) carbon fiber reinforced polymer (CFRP)-strengthened reinforced concrete (RC) beams. The experimental program included 11 beams, where the effect of the strengthening (CFRP) ratio (0.06 % and 0.18 %), fatigue load level (R1 = 0.57 and R2 = 0.38) and applied temperature (20 °C and 70 °C) have been considered. Experimental results on fatigue tests showed that high service temperature resulted in an increase in deflections and reduction in the stiffness of the specimens along the test. Moreover, the application of fatigue cycles with larger amplitude resulted in the failure of the specimens (by steel rupture), whilst specimens submitted to lower fatigue amplitude survived to the fatigue cycles. The NSM CFRP-strengthening helped to postpone the final failure of strengthened RC beams after steel reinforcement rupture during the fatigue test. Besides, damage due to fatigue derived in lower residual yielding and ultimate load in the post-fatigue test.

1. Introduction

Rehabilitation of civil structures needs attention in order to increase their lifetime and load-carrying capacity. These structures can be degraded by environmental factors and repeated loading (e.g. fatigue) that transfers to the structural members along a certain period and frequency [1–3]. Fatigue failure of a structural element is defined as a progressive cracking/damaging in the materials composing the element up to fracture under repeated loading. Unlike short-term loading, fatigue loading causes a reduction in stiffness of the system due to stress/strain accumulation in the materials that may lead to a failure in the system before reaching its ultimate capacity [3–5].

In the last decades, fiber-reinforced polymer (FRP) materials, available in different types and shapes, have been promoted to strengthen distressed structures. Nowadays, different techniques are used in FRP-strengthened structures, namely externally bonded reinforcement (EBR) and near-surface mounted (NSM) techniques [6], being the later the most recent one. In this technique, grooves are cut in the concrete surface and then the FRPs are inserted into these grooves using a proper adhesive. When compared to the EBR system, the NSM technique has several advantages such as: no need for surface treatment, less susceptible to environmental conditions, less prone to vandalism and good finished surface, among others [7,8].

Due to the nature of epoxy adhesives typically used in the NSM FRP-strengthening technique, their mechanical properties can be affected by the application of temperature variations or constant temperature approaching the glass transition temperature (T_g) of the adhesive [9–12]. Although a significant amount of work on the flexural behavior of NSM FRP-strengthened RC beams under short-term loading exists [7,8,13–17], few studies addressing the effect of high service temperature have been published [18–20].

Regarding the fatigue behavior of the FRP-strengthened RC beams, a significant amount of work has been done for the EBR FRP-strengthening system [21–29], whereas less literature exists for the case of NSM FRP-strengthening [30–34]. The fatigue behavior of RC beams strongly depends on the stress range in steel reinforcement. According to the literature, fatigue life decreases if the fatigue load level or/and the fatigue cycle amplitude are increased [25,26,30,32], and vice versa [33,34].

Existing studies confirm that fatigue life of EBR CFRP-strengthened beams is higher, when compared to unstrengthened control beams, because of the relief of stresses in internal steel reinforcement [21].

* Corresponding author.
E-mail address: marta.baena@udg.edu (M. Baena).

https://doi.org/10.1016/j.engstruct.2022.115119
Received 1 July 2022; Received in revised form 19 September 2022; Accepted 9 October 2022
Available online 25 October 2022

However, the inclusion of EBR CFRP-strengthening has no effect on failure mode, and unstrengthened and strengthened beams fail by steel reinforcement rupture [21–26], as a result of the stress/strain accumulation in the steel reinforcement. Steel rupture is occasionally followed by a deboning of FRP laminate from concrete surface. Focusing on the effect of environmental conditions on the fatigue performance, fatigue life of EBR CFRP-strengthened specimens is reduced when subjected to the hot-wet environmental conditions [27], and any increase in the corrosion degree (which is more common in old bridge structures) results in a reduction in the fatigue life in both strengthened and unstrengthened beams [28]. Moreover, the effect of temperature was studied in [29], where the application of 50 °C had no effect on the fatigue behavior of EBR CFRP-strengthened specimens. However, their post fatigue residual strength slightly improved due to possible post-curing in the epoxy adhesive at that temperature [29].

Similarly, results on the fatigue performance of NSM FRP-strengthened RC elements confirm the extension in fatigue life of strengthened specimens and the steel reinforcement rupture failure mode [30–32]. However, unlike EBR systems, no debonding occurred after steel rupture [35]. In fact, NSM technique has shown better fatigue performance than EBR technique in those cases where comparative studies have been performed [35–37]. Finally, different types of NSM bars and strips [30–32] and bonding material [33] have been considered in the evaluation of the fatigue behavior of NSM FRP-strengthened RC elements. In this sense, for a given level of load, sandblasted rods performed better than spirally wound rods [31], and strips performed even better [32]. Besides, a better fatigue performance was observed when cementitious adhesives were used, in comparison to epoxy adhesives, and this was attributed to the better bond and stress transfer between the CFRP strips and concrete [33].

According to the literature, there is a significant amount of work in evaluating the effect of fatigue loading on the performance of EBR FRP-strengthened RC beams, that reduces when we focus on NSM FRP-strengthened RC elements. Besides, to the best of authors knowledge, the analysis on the effect of high service temperature on the fatigue response of NSM carbon FRP (CFRP) strengthened RC beams has not been addressed yet. In this work, an experimental program to investigate the fatigue behavior of NSM CFRP-strengthened RC beams subjected to room temperature (20 °C) and high service temperature (70 °C) is presented. To this end, a total of 11 beams were tested where different parameters were considered: (i) CFRP strengthening ratio, (ii) testing temperature and (iii) fatigue load range. The fatigue tests were programed up to 2 million cycles if failure does not occur before, with a frequency of 2 Hz. Experimental results are presented and discussed in terms of instantaneous load–deflection response of the reference beams, cyclic load–deflection response and evolution of deflection, stiffness, concrete strain and dissipated energy along fatigue cycles. Finally, post-fatigue behavior of the beams and failure modes are also analyzed.

2. Experimental program

2.1. Materials

2.1.1. Concrete

All the beams were casted using the same batch of ready-mix concrete in lab conditions with conventionally vibrating procedure. The cement type was II-42.5R, with a content of 320 kg/m^3, the maximum aggregate size was 12 mm, and the water/cement ratio was 0.5. To improve concrete workability, a viscosity modifier was used. The experimental compressive strength (f_c), tensile strength (f_t), and modulus of elasticity (E_c) of concrete were determined at different ages of concrete at room temperature, so that concrete properties were tracked along the whole experimental campaign. To this end, cylinder specimens with 300 mm nominal height and 150 mm nominal diameter were used to determine the f_c, f_t, and E_c according to UNE-EN 12390–3:2003 [38], UNE-EN 12390–6:2010 [39], and ASTM C469-87 [40] standards, respectively. For each test, three specimens were used. Concrete mechanical properties at different ages are shown in Table 1.

Table 1
Concrete mechanical properties.

Concrete age (days)	Compressive strength, f_c (MPa)	Tensile strength, f_t (MPa)	Modulus of elasticity, E_c (GPa)
31	32.2 (2.2 %)[b]	3.1 (1.2 %)[b]	37.7 (4.2 %)[b]
107[a]	40.7 (2.2 %)[b]	3.5 (6.8 %)[b]	38.0 (5.6 %)[b]
150	41.1 (2.5 %)[b]	3.8 (3.6 %)[b]	39.9 (3.8 %)[b]
204	41.4 (4.8 %)[b]	3.7 (8.3 %)[b]	39.0 (7.6 %)[b]

[a]Age at first fatigue test.
[b]Coefficient of variation (CoV).

Table 2
Tensile mechanical properties of steel bars.

Bar diameter (mm)	Yielding stress f_y (MPa)	Ultimate stress, f_u (MPa)	Modulus of elasticity, E_s (GPa)
6	553.8 (1.6 %)[a]	703.5 (1.9 %)[a]	203.6 (0.8 %)[a]
8	536.7 (3.3 %)[a]	698.1 (1.9 %)[a]	196.4 (3.0 %)[a]
10	544.1 (2.9 %)[a]	666.0 (1.6 %)[a]	202.1 (5.5 %)[a]

[a]Coefficient of variation (CoV).

2.1.2. Steel reinforcement

In this work, ribbed steel bars with a diameter of 6 mm, 8 mm and 10 mm were used. The tensile mechanical properties of steel bars were obtained from tension tests based on UNE-EN ISO 15630-1 [41]. For each diameter, three samples were tested. Results on the yielding stress (f_y), the ultimate stress (f_u) and the modulus of elasticity (E_s) are reported in Table 2.

2.1.3. CFRP strips

CFRP strips, consisting of unidirectional carbon fibers (with a volume content fiber higher than 68 %) held together by an epoxy vinyl ester resin matrix, were used for strengthening the specimens [42]. The CFRP strips had a cross-section of 1.4 × 10 mm and their tensile mechanical properties were obtained from five CFRP samples, according to ISO 527-5 [43] recommendations. An ultimate tensile strength ($f_{u,FRP}$) of 2251.4 MPa (CoV = 3.2 %), an ultimate tensile strain ($\varepsilon_{u,FRP}$) of 0.0133 (CoV = 7.2 %), and a modulus of elasticity (E_{FRP}) of 169.5 GPa (CoV = 6.3 %) were obtained [18].

2.1.4. Epoxy adhesive

In this study, a high performance, solvent-free, thixotropic, and grey two-component epoxy adhesive specially developed for bonding CFRP to concrete was used. According to the manufacturer's product data sheet [44], the components A (resin) and B (hardener) should be mixed at a ratio of 2:1 by weight. The glass-transition temperature (T_g) of epoxy was determined by differential scanning calorimetry (DSC) [45] and dynamic mechanical analysis (DMA) [46]. The epoxy specimens were tested after a curing time at lab conditions of 12 days. According to test results, the T_g of epoxy was in the range of 53.9–65.3 °C [18].

Tensile strength ($f_{u,epoxy}$) and modulus of elasticity (E_{epoxy}) of the epoxy adhesive were determined by testing dog-bone specimens following ISO-527–1 [47] specifications. Furthermore, in order to evaluate the effect of temperature on mechanical properties of the epoxy adhesive, characterization tests were performed at 20 °C and 70 °C. The mechanical properties of epoxy adhesive are summarized in Table 3 [9].

2.2. Test program and configuration

The experimental program included 11 beams divided into two series, where the effect of different parameters was studied, namely: (i) strengthening ratio (i.e. one and three CFRP strips), (ii) temperature (i.e. 20 and 70 °C) and (iii) R ratio (i.e. 0.57 and 0.38). In this sense, R ratio is

Table 3
Mechanical properties of epoxy adhesive tested at different temperatures [9].

Testing temperature (°C)	$f_{u,epoxy}$ (MPa)	$f_{u,epoxy-70}/f^{a}_{u,epoxy-20}$	E_{epoxy} (MPa)	$E_{epoxy-70}/E^{a}_{epoxy-20}$
20	28.0 (0.4 %)[b]	–	8102.4 (0.8 %)[b]	–
70	2.7 (3.7 %)[b]	0.1	271.5 (4.8 %)[b]	0.03

[a]Defined as the ratio between the property value at 70 °C and the reference property value at 20 °C.
[b] Coefficient of variation (CoV).

Table 4
Test matrix.

Series	Group	Beam ID	Age of concrete [a] (days)	No. of CFRP strips	CFRP area (mm^2)	Testing Temperature (°C)	R ratio
Series 1	–	CB-20-ST	104	–	–	20	–
		SB1S-20-ST	138	1	14		–
		SB3S-20-ST	170	3	42		–
Series 2	Group 1	CB-20-R1	107	–	–	20	0.57
		SB1S-20-R1	142	1	14		0.57
		SB3S-20-R1	171	3	42		0.57
		SB3S-20-R2	199	3	42		0.38
	Group 2	CB-70-R1	126	–	–	70	0.57
		SB1S-70-R1	158	1	14		0.57
		SB3S-70-R1	184	3	42		0.57
		SB3S-70-R2	206	3	42		0.38

[a]Age of concrete at the beginning of fatigue test.

defined as the ratio between minimum load and maximum load of the fatigue cycle. In Series 1, three beams were considered as reference beams to be tested under short-term loading in order to define the fatigue load level to be applied to beams in Series 2 (see Table 4). Among these three reference beams, one beam was unstrengthened and the other two beams were strengthened with one and three CFRP strips, respectively. All beams in Series 1 were tested at 20 °C. In Series 2, eight beams were tested under different fatigue loading levels and

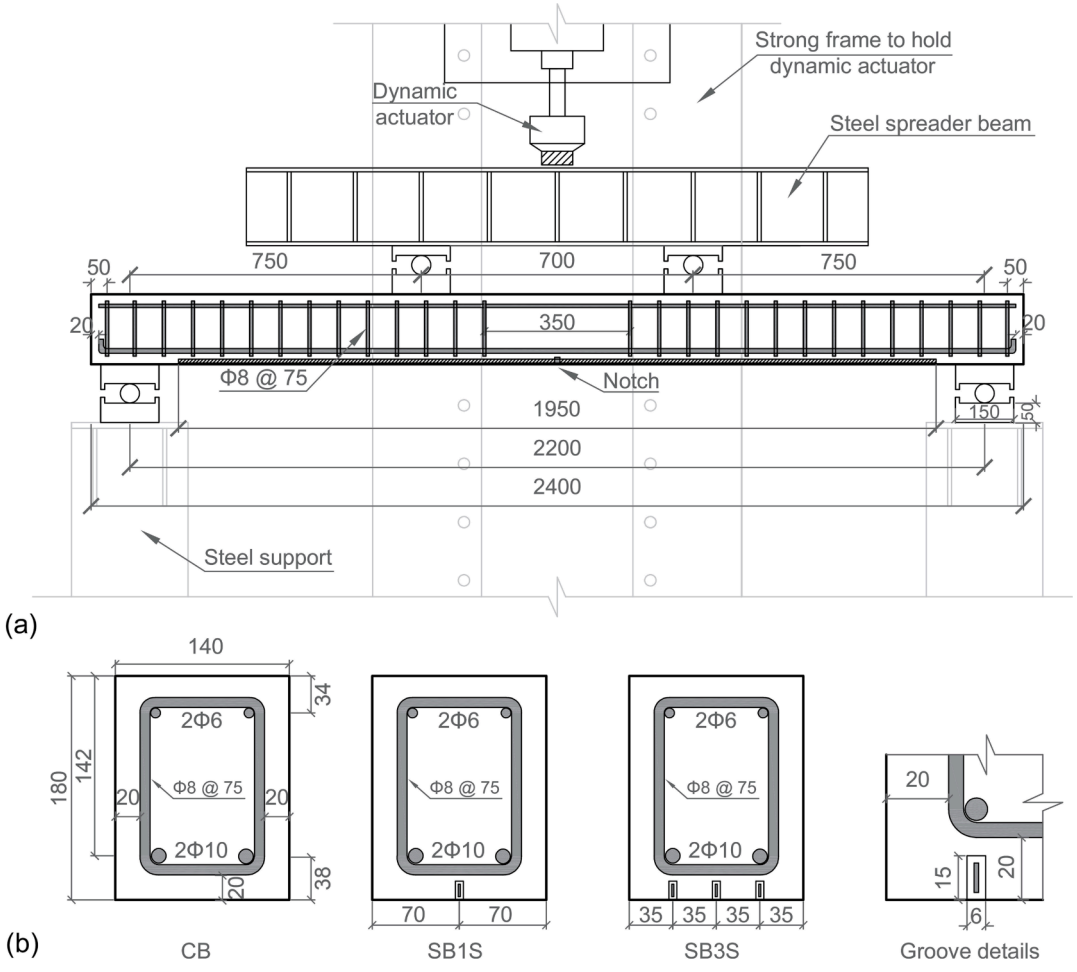

Fig. 1. Four-point bending test configuration: (a) Test setup and (b) Cross-section details (all dimensions in mm).

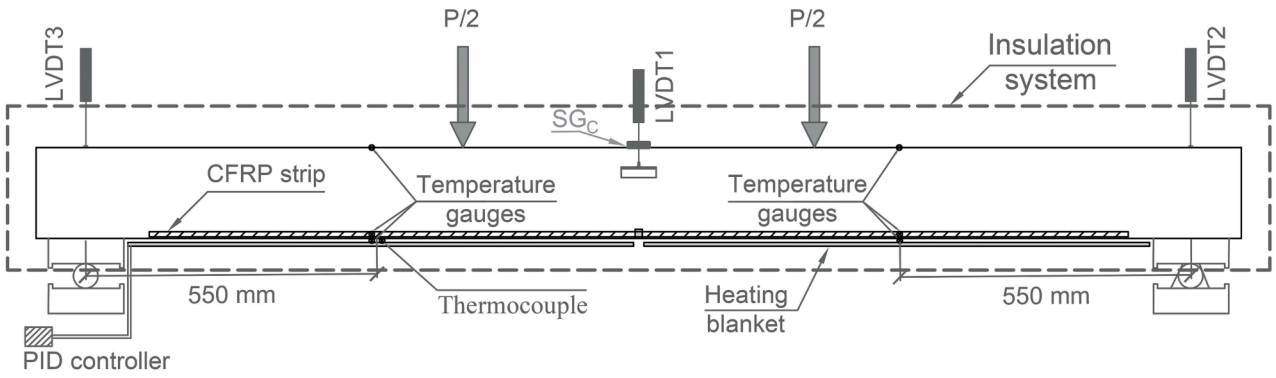

Fig. 2. Instrumentation adapted in the beams.

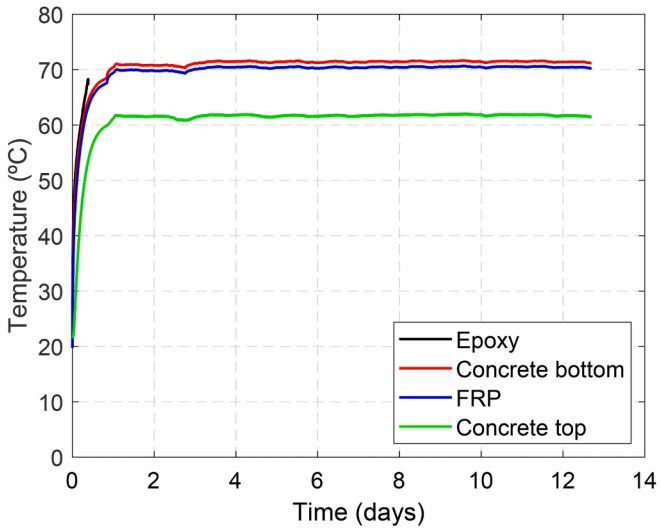

Fig. 3. Registered temperatures during the heating process and the fatigue test; Note: temperature gauge on epoxy surface failed during the heating phase.

temperatures. This series was divided into two groups, according to the temperature applied during the fatigue test (Groups 1 and 2 refer to beams tested at 20 °C and 70 °C, respectively). Each of these two groups included four beams, three of them tested with a R ratio equal to 0.57 and one of them with an R ratio equal to 0.38 (see Table 4).

The fatigue load level was defined based on the yielding stress of the reinforcing steel (f_y) of the reference beams under short-term loading (Series 1). In this sense, for the fatigue level R1, the minimum fatigue load (P_{min}) and the maximum fatigue load (P_{max}) were those causing the stress in reinforcing steel to be equal to 40 % and 70 % of its yielding stress (f_y) at the corresponding reference beam, respectively, which led to a R ratio equal to 0.57. For the fatigue level of R2, this range was between 30 % and 80 % of f_y of the corresponding reference beam, respectively, which led to a R ratio equal to 0.38. The maximum load was limited to be less than the load causing 80 % of steel yielding stress (f_y), according to ACI 440.2R [48].

Specimens' designation reads X-Y-Z, where X denotes the type of beam (CB standing for control beam, and SB1S and SB3S referring to beams strengthened with one and three CFRP strips, respectively). Furthermore, Y stands for the testing temperature. Finally, Z indicates the loading type (ST standing for short-term loading, and R1 and R2 referring to fatigue loading with different R ratios). For instance, CB-20-ST, refers to the control beam tested at 20 °C under short-term loading. Furthermore, SB3S-70-R1 refers to a beam strengthened with three

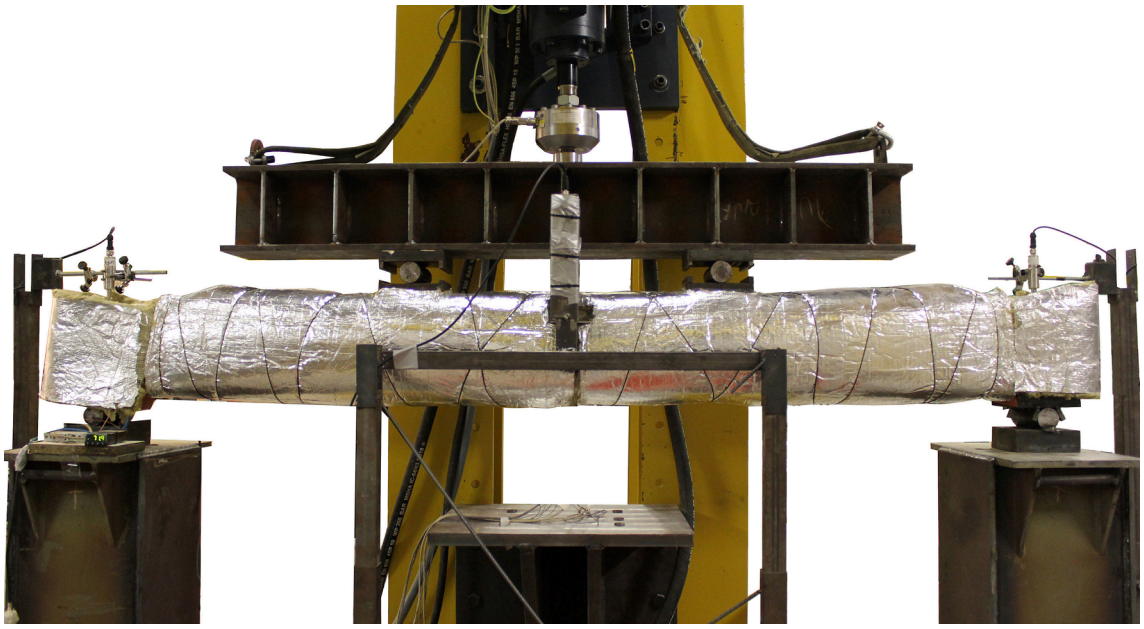

Fig. 4. General view of test setup.

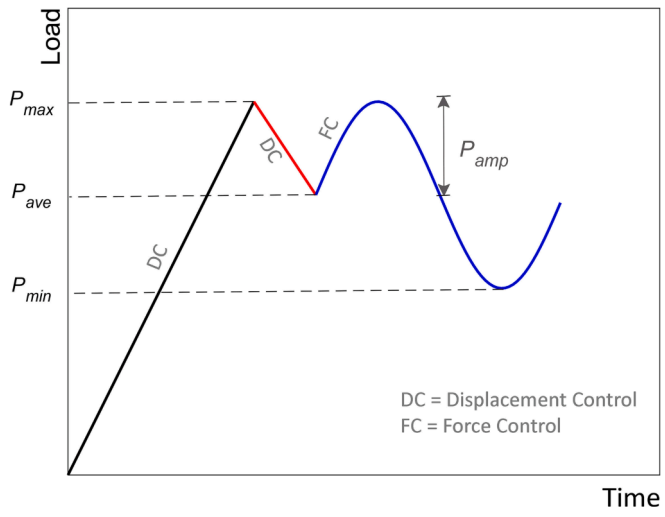

Fig. 5. Fatigue loading procedure.

CFRP strips and tested at 70 °C under fatigue loading with R = 0.57.

The beams were tested under a four-point bending test configuration (see Fig. 1). The beams were 2400 mm long (clear span of 2200 mm), 140 mm wide and 180 mm deep. The loading span and shear span were 700 mm and 750 mm, respectively. Two longitudinal steel bars with 10 mm of diameter (2Φ10) were used in the tension side of the beam, resulting in a reinforcement ratio of 0.79 %. Moreover, 2Φ6 were used in the compression side of the beams. All beams had shear reinforcement consisting of steel stirrups with a diameter of 8 mm placed every 75 mm. In the strengthened beams, CFRP strips with a cross-section of 1.4 × 10 mm and a bonded length of 1950 mm were used. In order to mount the CFRP strips, grooves with dimensions of 6 × 15 mm were cut in the soffit of the beams. In those beams were more than one groove was needed the distance between grooves was set based on fib Bulletin 90 [49] recommendations. Finally, during the cutting of the grooves, a notch (5 mm wide and 15 mm deep) was created at midspan in order to act as a crack initiator.

2.3. Instrumentation

The instrumentation used for the presented experimental work is shown in Fig. 2. A linear vertical displacement transducer (LVDT) with 100 mm stroke (with linearity error of ± 0.10 % F.S.) was used in the midspan of the beam to measure the central deflection (LVDT1). Moreover, two LVDTs with 25 mm stroke (with linearity error of ± 0.10 % F.S.) were used in both support (LVDT2 and LVDT3) in order to measure the possible supports settlement in all of the tests. Furthermore, the strain at the top fiber of concrete was measured with a strain gauge (with a gauge length of 60 mm) that was installed in midspan of the specimens (SG_C in Fig. 2). Finally, a load-cell of 125 kN was used to register the applied load.

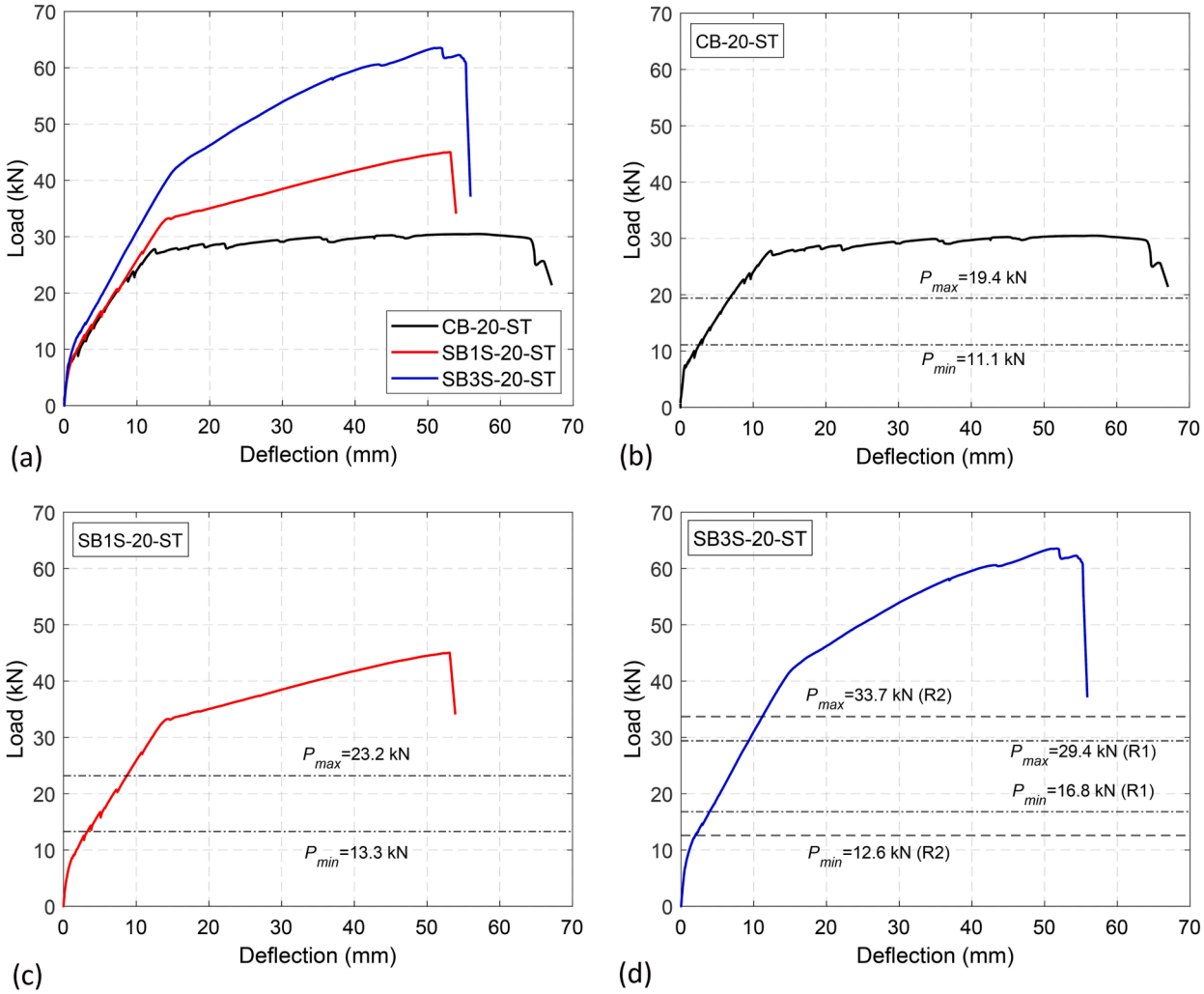

Fig. 6. Short-term load–deflection curves (Series 1): (a) Effect of strengthening ratio; (b), (c) and (d) definition of P_{max} and P_{min}.

Table 5
Details on fatigue load levels.

Specimen ID	P_y[a] (kN)	P_{min} (kN)	P_{max} (kN)	P_{ave}[b] (kN)	P_{amp}[c] (kN)	R[d]
CB-20-R1 CB-70-R1	27.7	11.1	19.4	15.3	4.1	0.57
SB1S-20-R1 SB1S-70-R1	33.1	13.3	23.2	18.3	4.9	0.57
SB3S-20-R1 SB3S-70-R1	41.9	16.8	29.4	23.1	6.3	0.57
SB3S-20-R2 SB3S-70-R2	41.9	12.6	33.7	23.1	10.6	0.38

[a] P_y of the reference short-term test in Series 1.
[b] Average fatigue load defined as: $P_{ave} = (P_{max} + P_{min})/2$.
[c] Amplitude of fatigue cycles defined as: $P_{amp} = P_{max} - P_{ave}$.
[d] $R = P_{min}/P_{max}$.

Some specimens needed to be conditioned (i.e. heated up to 70 °C) prior to fatigue testing. In those cases, heating blankets installed to the soffit of the beams were used. A proportional integral derivative (PID) controller was utilized for controlling heating process, and Type-T thermocouples, installed between the heating blanket and the soffit of the beam, were used as temperature controller sensor. An isolation system (rock wool with aluminum foil) was used in order to speed up the heating process and reach to a uniform temperature along the beam. Temperature gauges were used to monitor and register temperature at different points: on the concrete surface at the top and bottom of the beam, on the surface of the CFRP and on the surface of epoxy adhesive (see Fig. 2). The temperature gauges on the surface of the CFRP were installed prior to introducing the strip into the groove, and a thin protection layer was applied in order to protect them from the wet environment during curing of the epoxy adhesive. The heating process started almost 24 h prior to fatigue testing until the average temperature in the soffit of the beam was stabilized to its target value. During fatigue testing, the PID controller ensured the temperature to be constant along the test. The evolution of the temperature during the heating process and the fatigue test of one of the beams is shown in Fig. 3. Although there was a small difference between temperature at the concrete top and concrete bottom, the temperature gradient did not affect the

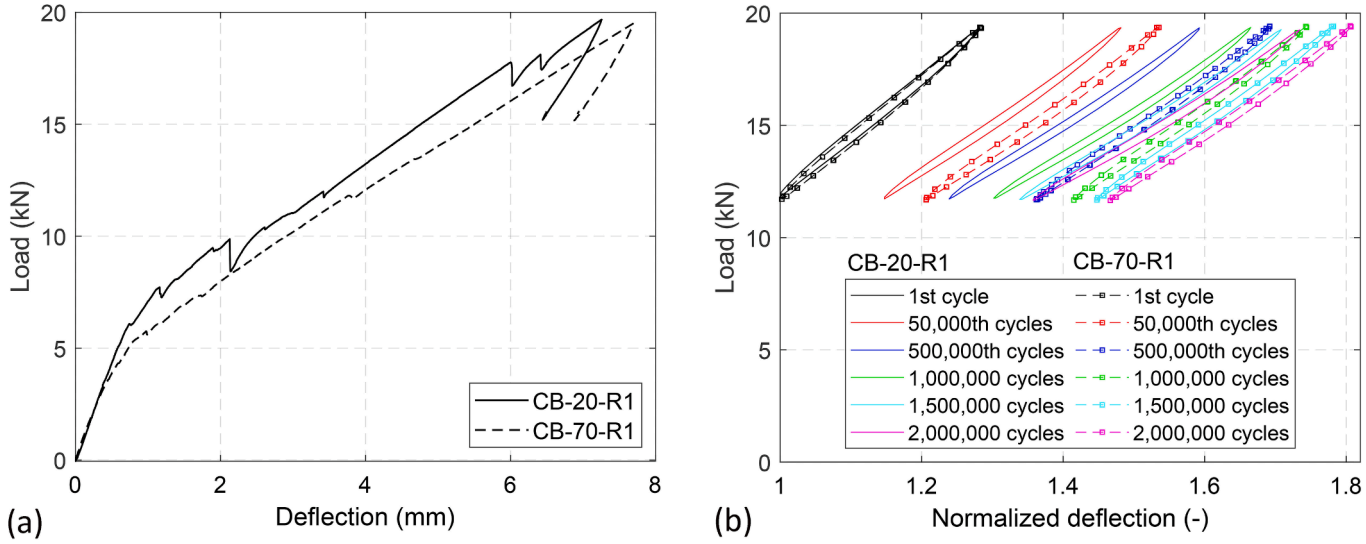

Fig. 7. Fatigue response of specimens CB-20-R1 and CB-70-R1: (a) Initial load–deflection response prior to cyclic loading, and (b) load versus normalized deflection curves during cyclic loading.

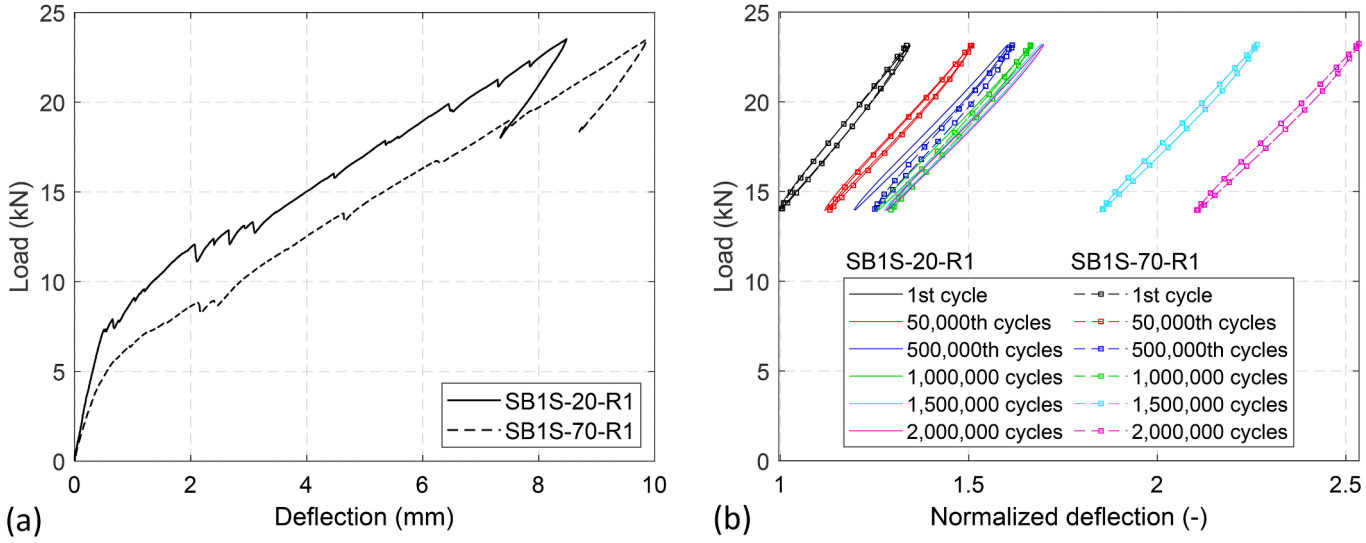

Fig. 8. Fatigue response of specimens SB1S-20-R1 and SB1S-70-R1: (a) Initial load-deflection response prior to cyclic loading, and (b) load versus normalized deflection curves during cyclic loading.

outcome of the research carried out. In addition, a general view of test setup for a beam under temperature is shown in Fig. 4.

2.4. Loading procedure

Specimens in Series 1 were tested under short-term load under displacement control at a rate of 0.6 mm/min up to failure. As mentioned before, these specimens were used to define the maximum and minimum fatigue loads (P_{max} and P_{min}, respectively) of specimens in Series 2. The fatigue tests were performed in three different steps as below (see Fig. 5):

- Step 1: The beams were loaded up to the maximum fatigue load (P_{max}) under displacement control at a rate of 0.6 mm/min (black line in Fig. 5).
- Step 2: The beams were unloaded up to the average fatigue load ($P_{ave} = (P_{max} + P_{min})/2$) under displacement control at a rate of 0.6 mm/min (red line in Fig. 5).
- Step 3: In this step, the fatigue load was applied through a sinusoidal loading path with a frequency of 2 Hz and a pre-defined amplitude ($P_{amp} = P_{max} - P_{ave}$). This step was conducted under force control. The fatigue test duration was programmed to either 2 million cycles or failure of the beam, whichever occurs first (blue line in Fig. 5).

3. Results and discussions

3.1. Short-term tests results

The results of specimens of Series 1 (short-term test) (i) allowed the definition of the fatigue loads (P_{max} and P_{min}) to be applied to specimens in Series 2 and also (ii) were used for comparison purposes with results obtained on the specimens that experienced the post-fatigue stage. Experimental load-midspan deflection curves of specimens in Series 1 are shown in Fig. 6, where three phases can be observed: (i) uncracked phase, with a linear elastic behavior until cracking load (P_{cr}) is attained; (ii) cracking phase, where stiffness gradually decreases as the load increases up to the yielding of steel reinforcement; and (iii) post-yielding

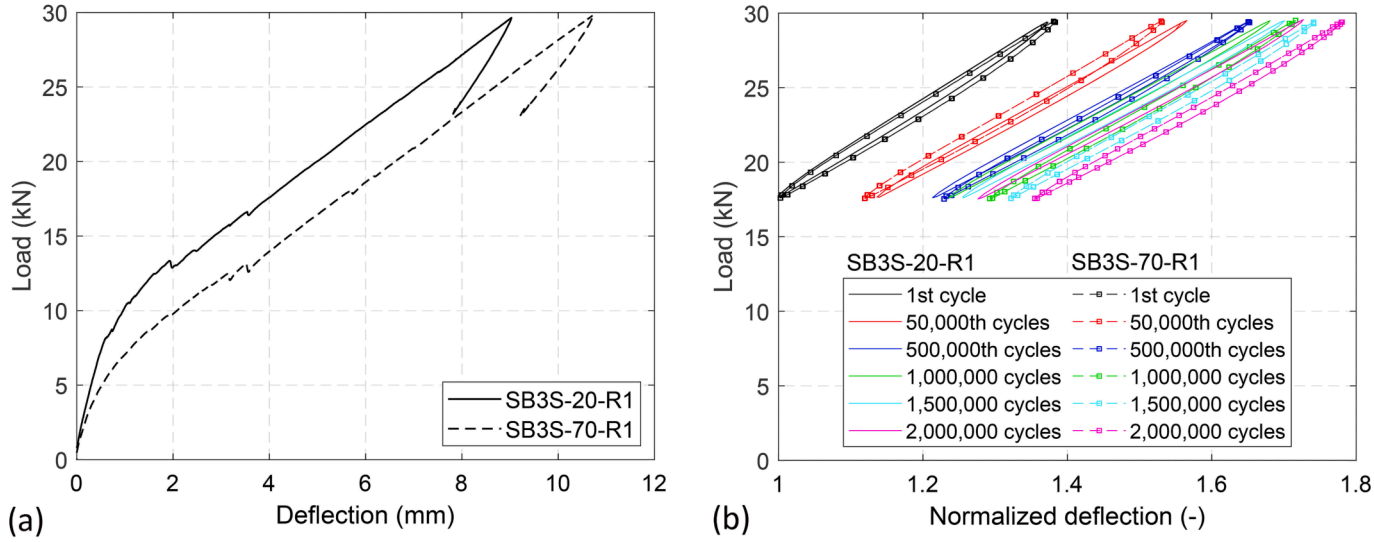

Fig. 9. Fatigue response of specimens SB3S-20-R1 and SB3S-70-R1: (a) Initial load-deflection response prior to cyclic loading, and (b) load versus normalized deflection curves during cyclic loading.

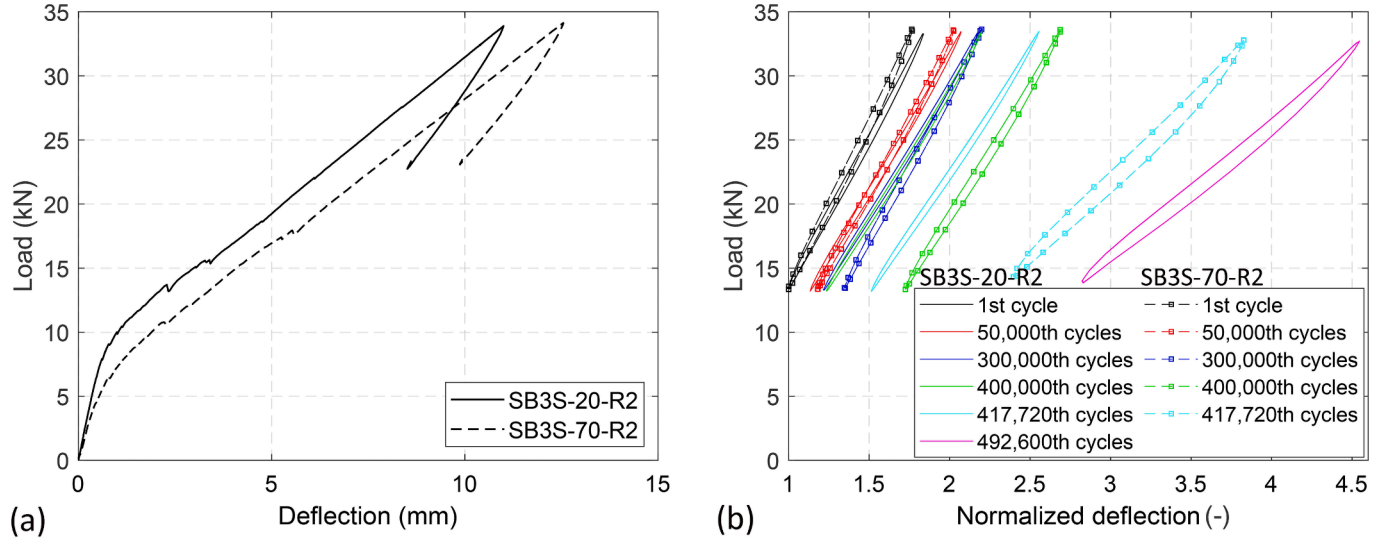

Fig. 10. Fatigue response of specimens SB3S-20-R2 and SB3S-70-R2: (a) Initial load–deflection response prior to cyclic loading, and (b) load versus normalized deflection curves during cyclic loading.

phase up to failure. In this last phase no significant increase in load can be observed for the unstrengthened beam, whilst relevant load increase is observed for strengthened beams. The increase in the strengthening (CFRP) ratio had no significant effect on the cracking load (P_{cr}), whilst larger yielding load (P_y) and ultimate load (P_u) were obtained in the specimen with larger strengthening ratio, as expected (see Fig. 6a). In this sense, the yielding and ultimate loads of specimen SB1S-20-ST were 20 % and 47 % larger than those of specimen CB-20-ST, while for the specimen with three strips (SB3S-20-ST) the percentages rose up to 51 % and 108 %, respectively. Finally, it should be mentioned that the unstrengthened beam failed by concrete crushing, whilst specimens strengthened with one and three laminates failed by CFRP rupture and intermediate concrete cover separation, respectively. Further discussion about the failure modes is provided in Section 3.4.

3.2. Fatigue tests results

Values for P_{min} and P_{max} applied to fatigue tests of specimens in Series 2 are depicted in Fig. 6b-6d and summarized in Table 5. It should be mentioned that P_{min} and P_{max} computed from results on short-term tests at 20 °C were applied to fatigue tests at both testing temperatures (20 °C and 70 °C).

3.2.1. Cyclic load-deflection response

Cyclic load-deflection responses of specimens in Series 2 are shown in Figs. 7-10. In every figure, two graphs are presented. Fig. 7a-10a correspond to the initial load–deflection response before cyclic loading (steps 1 and 2 of the fatigue loading procedure presented in section 2.4), and Fig. 7b-10b correspond to the cyclic load versus normalized deflection (with respect to deflection of first cycle) curves (step 3 of the fatigue loading procedure described in section 2.4).

The effect of temperature on the flexural behavior prior to fatigue loading can be assessed in Fig. 7a-10a. In all the cases, the application of a high service temperature (70 °C) resulted in lower cracking loads (P_{cr}) and an increase in the deflection prior to fatigue loading. In this sense, a comparison of the deflections prior to fatigue loading is presented in Fig. 11, where the greatest effect of temperature corresponds to specimen strengthened with three strips (SB3S-20-R1 vs SB3S-70-R1). On the other hand, unstrengthened control beams (CB-20-R1 and CB-70-R1) show the lowest variation. This behavior could be partially attributed to lower P_{cr} values, and therefore lower M_{cr} (i.e. cracking moment), leading to lower M_{cr}/M ratios which are related to larger deflections. Besides, a possible reduction in the effectiveness of the strengthening system due to the application of a working temperature beyond the T_g of the epoxy adhesive can also be affecting. This may be related to a reduction in the stiffness of the epoxy adhesive [50].

The effect of cyclic loading and temperature on the flexural response of specimens in Series 2 can be assessed in Fig. 7b-10b, where the cyclic load versus normalized deflection curves are plotted. In these subfigures, solid lines correspond to specimens tested at 20 °C while dashed lines refer to specimens tested at 70 °C. In all the cases, normalized deflections increased gradually as the fatigue loading progressed, and larger increments were found in specimens tested at 70 °C, which is in line with results presented in [27]. It is worth to mention that a large portion of fatigue deflections occurred at first 50,000 cycles and after that, the rate of deflection increase slowed down, as observed in [1,2,23,24,33,34].

Moreover, specimens tested under an R ratio equal to 0.57 (i.e. R1) did not fail during the application of 2 million cycles. However, special attention should be given to specimen SB1S-70-R1, which experienced a large jump in the normalized deflection at about 1.5 million cycles (see Fig. 8b). This jump was attributed to a reduction in the effectiveness of the strengthening system that may be due to the reduction in mechanical properties of epoxy adhesive at higher temperature. In this scenario, the value of P_{max} applied to SB1S-70-R1 (P_{max} = 23.2 kN) was larger than the load causing 80 % of steel yielding stress (f_y) of the control beam CB-20-ST, thus exceeding the limitation proposed by ACI 440.2R [48]. As a consequence, a possible accumulation of damage in steel reinforcement may have occurred.

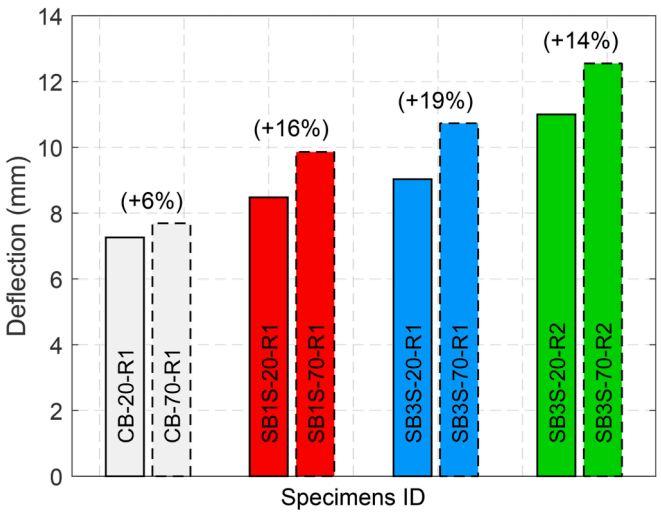

Fig. 11. Initial deflections prior to cyclic loading; Note: percentages refer to the variation in the deflection due to the effect of temperature.

On the other hand, specimens tested under an R ratio equal to 0.38 (i.e. R2) did not survive the programmed 2 million cycles and failed by steel reinforcement rupture. It should be mentioned that once rupture of the steel reinforcement took place, the integrity of the system was provided by the NSM CFRP-strengthening strips. In this sense, for specimen SB3S-20-R2 the steel reinforcement rupture took place at 411,220 cycles, and after that the NSM CFRP-strengthening was involved alone in order to resist the fatigue loading; from this point on, large increases in the curvature (deflection) occurred and the beam failed at 492,600 cycles. In the case of specimen under temperature (i.e. SB3S-70-R2), rupture of steel reinforcement took place at 340,890 cycles and the beam failed at 417,720 cycles. Therefore, NSM CFRP-strengthening improved the fatigue life of the system by 20 % and 22.5 % for SB3S-20-R2 and SB3S-70-R2, respectively. Besides, the application of temperature (70 °C) shortened the fatigue life of the specimen by 15 % (compare the fatigue life of SB3S-20-R2 and SB3S-70-R2).

Results on fatigue tests at specific number of cycles are reported in Table 6.

3.2.2. Average normalized deflection

With the aim at analyzing the evolution of deflection due to fatigue, the average normalized deflection, $\delta_{ave,n}$, has been defined as the average value of deflections corresponding to P_{min} and P_{max} in each cycle normalized with respect to the value at first cycle (i.e. the value of δ_{ave} for first cycle reported in Table 6). The evolution of $\delta_{ave,n}$ along fatigue loading is shown in Fig. 12. According to results presented in Fig. 12a, the presence of NSM CFRP-strengthening helped to reduce the detrimental effects of fatigue loading and, thus, lower values of $\delta_{ave,n}$ were obtained. Furthermore, the application of a high service temperature (70 °C) negatively affected the fatigue performance of both unstrengthened and strengthened specimens. Besides, the large jump in deflection taking place in specimen SB1S-70-R1 at around 1.5 million cycles is clearly visible in Fig. 12a (see red dash line in Fig. 12a). The effect of R ratio on $\delta_{ave,n}$ can be analyzed from results presented in Fig. 12b. In this case, although similar patterns were obtained during the initial cycles of the fatigue tests, specimens under lower R ratios failed by steel rupture and experienced a sudden increase in $\delta_{ave,n}$ prior to final failure (see green lines in Fig. 12b). The failure in these specimens can be explained by the combination of having a lower R ratio and a larger maximum fatigue load, P_{max}, that in this case was equal to the upper limit stated in ACI 440.2R [48]. This is in accordance with

Table 6
Fatigue tests results.

Specimens ID	Fatigue life (cycles)	Failure mode [a]	$E^{b}_{tot,acc,diss}$ (kN·m)	Cycle	δ^{c}_{ave} (mm)	K^{d} (kN/mm)	ε^{e}_{ave} (με)
CB-20-R1	>2,000,000	Not failed	1432	1	6.5	4.6	−718
				50,000	7.5	4.0	−778
				500,000	8.1	3.7	−867
				1,000,000	8.5	3.7	−907
				1,500,000	8.7	3.6	−937
				2,000,000	8.8	3.5	−968
CB-70-R1	>2,000,000	Not failed	1462	1	7.0	4.4	−775
				50,000	8.5	3.8	−887
				500,000	9.4	3.8	−1051
				1,000,000	9.7	3.8	−1152
				1,500,000	9.9	3.8	−1200
				2,000,000	10.1	3.7	−1229
SB1S-20-R1	>2,000,000	Not failed	1991	1	7.3	4.2	−646
				50,000	8.2	3.8	−691
				500,000	8.7	3.6	−751
				1,000,000	9.1	3.6	−803
				1,500,000	9.3	3.6	−829
				2,000,000	9.3	3.6	−864
SB1S-70-R1	>2,000,000	Not failed	2394	1	8.5	3.8	−741
				50,000	9.6	3.4	−838
				500,000	10.4	3.4	−982
				1,000,000	10.7	3.4	−1061
				1,500,000	14.9	3.1	−1113
				2,000,000	16.8	3.0	−1164
SB3S-20-R1	>2,000,000	Not failed	2845	1	7.9	4.7	−700
				50,000	9.1	4.1	−771
				500,000	9.6	4.0	−858
				1,000,000	9.8	4.0	−888
				1,500,000	9.9	4.0	−905
				2,000,000	10.1	4.0	−931
SB3S-70-R1	>2,000,000	Not failed	3375	1	9.1	4.1	−887
				50,000	10.1	3.8	−1030
				500,000	11.1	3.7	−1204
				1,000,000	11.5	3.7	−1295
				1,500,000	11.7	3.7	−1369
				2,000,000	12.0	3.6	−1405
SB3S-20-R2	492,600	SR	1933	1	8.4	4.0	−657
				50,000	9.5	3.6	−708
				300,000	10.1	3.5	−753
				400,000	10.2	3.5	−761
				417,720	12.1	3.3	−798
				492,600	21.9	1.6	−1127
SB3S-70-R2	417,720	SR	2266	1	9.9	3.7	−898
				50,000	11.5	3.3	−1027
				300,000	12.7	3.3	−1216
				400,000	15.8	2.9	−2178
				417,720	22.2	1.6	−2548

[a] SR = Steel reinforcement rupture.
[b] Total accumulated dissipated energy at the end of the fatigue test.
[c] Average deflection.
[d] Stiffness.
[e] Average concrete strain.

[25,26,30,32], who observed that the increase in P_{max} and/or the decrease in R ratio results in a reduction of fatigue life with specimens failing by steel rupture.

In order to clearly compare the effect of NSM CFRP strengthening ratio, temperature and R ratio on the average normalized deflection ($\delta_{ave,n}$), a bar diagram is presented in Fig. 13, where $\delta_{ave,n}$ is compared at three different cycles: i) at 417,720th cycle, where SB3S-70-R2 failed; ii) at 492,600th cycle, where SB3S-20-R2 failed and iii) at 2 million cycle, corresponding to the end of the fatigue test. The comparison of the first set of data (deflections at 417,720th cycle) shows that higher service temperature, applied individually to specimens having an R ratio of 0.57, had no significant effect at that number of cycles (specimen SB3S-20-R1 vs SB3S-70-R1), whereas the change to lower R ratios in specimens at 20 °C had a larger impact on the fatigue performance (specimen SB3S-20-R1 vs SB3S-20-R2). In fact, specimen SB3S-20-R2 had already experienced steel rupture at that cycle as a consequence of the high damage produced by P_{max}. Finally, the application of temperature and lower R ratios in a combined manner had catastrophic consequences, causing the failure of the beam (specimen SB3S-20-R1 vs SB3S-70-R2). Results of the second set of data (deflections at 492,600th cycle) confirm that R ratio had the major effect. Finally, the third set of data confirms that, for an R ratio equal to 0.57, the application of a high service temperature was affecting the fatigue performance of control and strengthened beams in a controlled manner. Special attention should be given to specimen SB1S-70-R1, which experienced and unexpected jump in deflections at 1.5 million cycles, as explained before.

3.2.3. Stiffness

Fatigue loading has an effect on the stiffness on any structural member, as it consists on a cyclic load being repeated for a long period of time. Thus, evaluation of the stiffness variation during a fatigue test is of paramount importance as the degradation in the stiffness may influence the serviceability of the strengthened system [1]. In this section, the evolution of stiffness along the fatigue loading is analyzed. To this end,

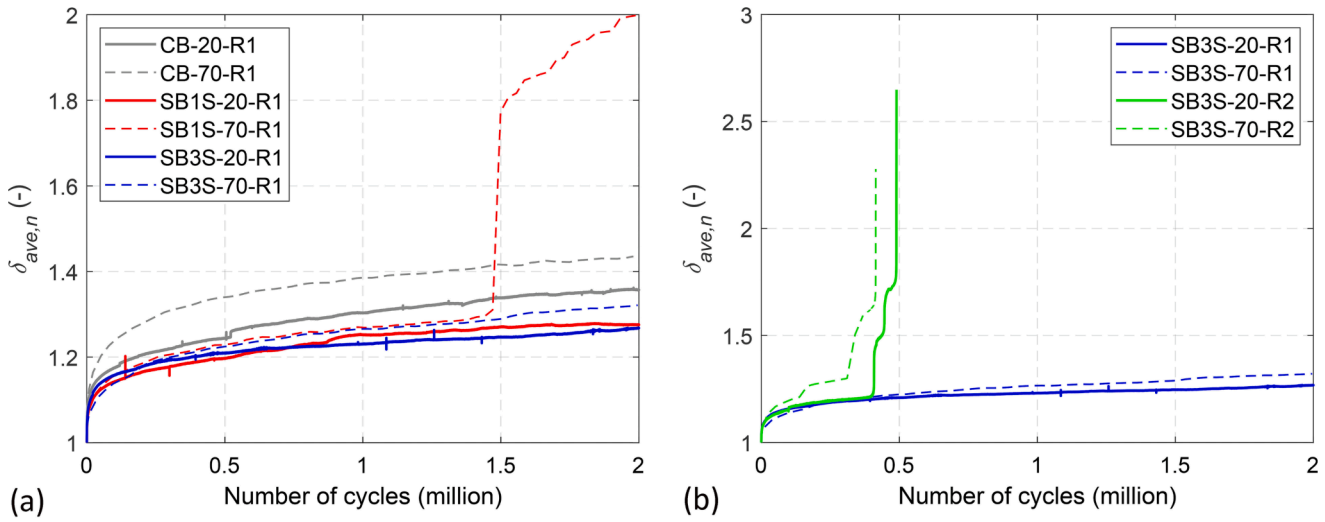

Fig. 12. Evolution of average normalized deflection ($\delta_{ave,n}$): (a) Effect of strengthening ratio and temperature; (b) Effect of R ratio and temperature in beams with same NSM CFRP-strengthening ratio.

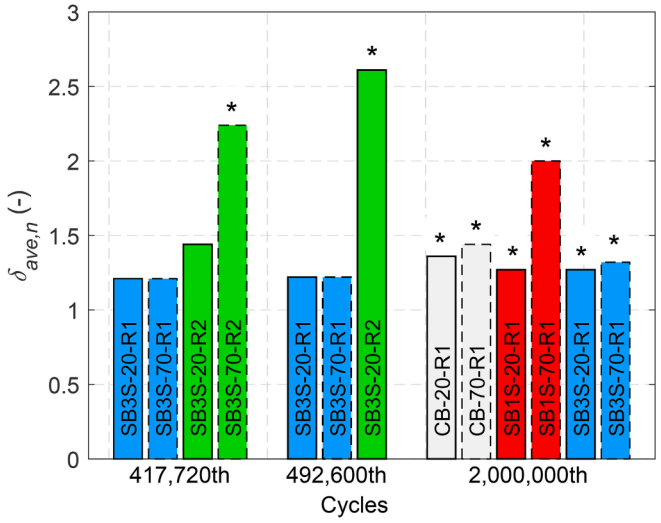

Fig. 13. Comparison of average normalized deflections ($\delta_{ave,n}$). *The value of average normalized deflection corresponds to the ultimate one ($\delta_{u,ave,n}$).

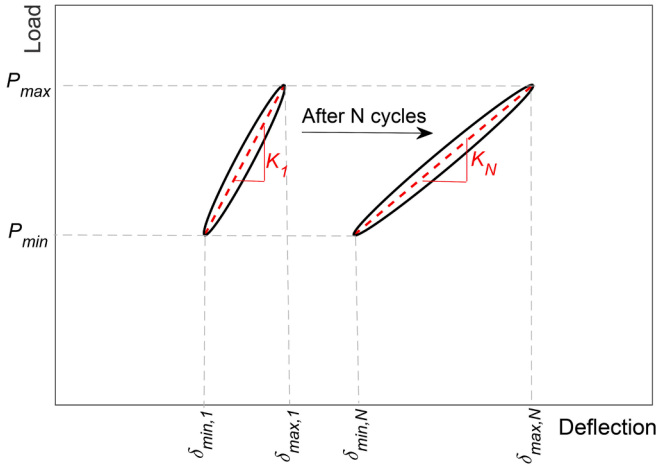

Fig. 14. Schematic view of stiffness calculation.

the stiffness (K) is calculated based on the behavior of the member within the loading and unloading paths of a cycle [24,33,34], as follows:

$$K_i = \frac{P_{max,i} - P_{min,i}}{\delta_{max,i} - \delta_{min,i}} \quad (1)$$

where $\delta_{max,i}$ and $\delta_{min,i}$ are the deflections corresponding to $P_{max,i}$ and $P_{min,i}$ at the ith cycle. A schematic view of this procedure is shown in red lines in Fig. 14.

The evolution of the stiffness (K) along the fatigue tests is shown in Fig. 15 and also reported in Table 6. According to experimental results, a big drop in stiffness happened during the first cycles, which corresponded to the increase in deflections shown in Fig. 12. Afterwards, stiffness tends to stabilize, with specimens tested at 20 °C showing larger stiffness than those tested at 70 °C. The same stiffness reduction tendency was observed in [27]. Besides, specimens under a larger R ratio showed larger stiffness (both unstrengthened and strengthened specimens), irrespective of the applied temperature. Furthermore, the increase in the strengthening ratio resulted in a higher stiffness in the specimens in comparison to unstrengthened control beams. The big drop in stiffness of specimen SB1S-70-R1 around the 1.5 million cycles corresponds to the big jump in deflection shown in Fig. 12a. Similarly, failure of specimens with low R ratio (i.e. R2 = 0.38) is visible in Fig. 15b.

3.2.4. *Average normalized concrete strain*

Measurements from the strain gauge on the top fiber of concrete (see Fig. 2) allow plotting the evolution of average normalized concrete strain ($\varepsilon_{ave,n}$), as presented in Fig. 16. Similar to the case of deflections, the average normalized concrete strain has been defined as the average value of concrete strain corresponding to P_{min} and P_{max} in each cycle normalized with respect to the value at first cycle (i.e. the value of δ_{ave} for first cycle reported in Table 6). According to experimental results, strengthening ratio did not have a considerable effect on the evolution of the normalized concrete strain along fatigue test. On the other hand, for the specimens under fatigue load level of R1, the increase in the testing temperature resulted in an increase of 20 % in the $\varepsilon_{u,ave,n}$ (see Fig. 16a). Finally, no significant differences can be found in the earlier stage of the evolution of average normalized concrete strain ($\varepsilon_{ave,n}$) whatever the R ratio is. However, specimens under low R ratio (i.e. R2 = 0.38) experienced a sudden increase in $\varepsilon_{ave,n}$ prior to the final failure (see Fig. 16b).

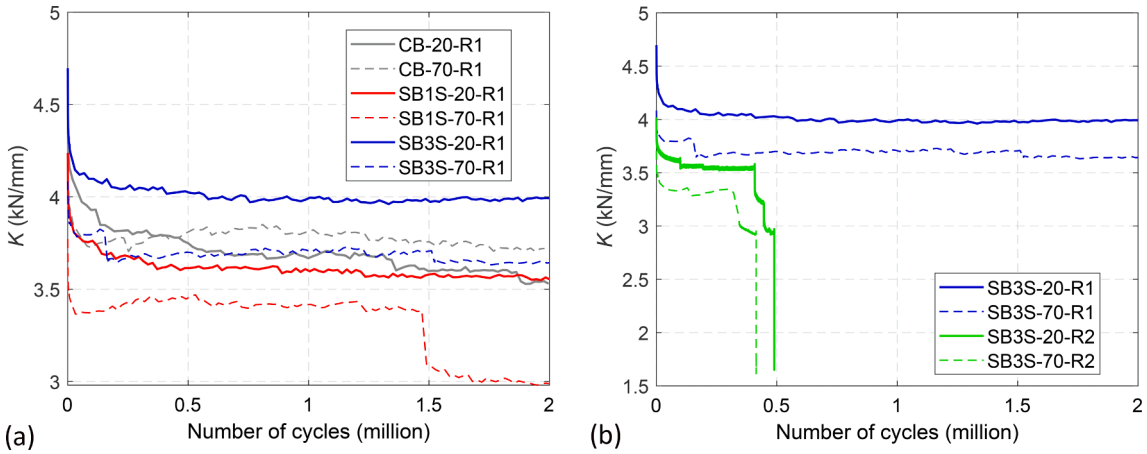

Fig. 15. Evolution of stiffness (K): (a) Effect of strengthening ratio and temperature and (b) Effect of R ratio and temperature in beams with same NSM CFRP-strengthening ratio.

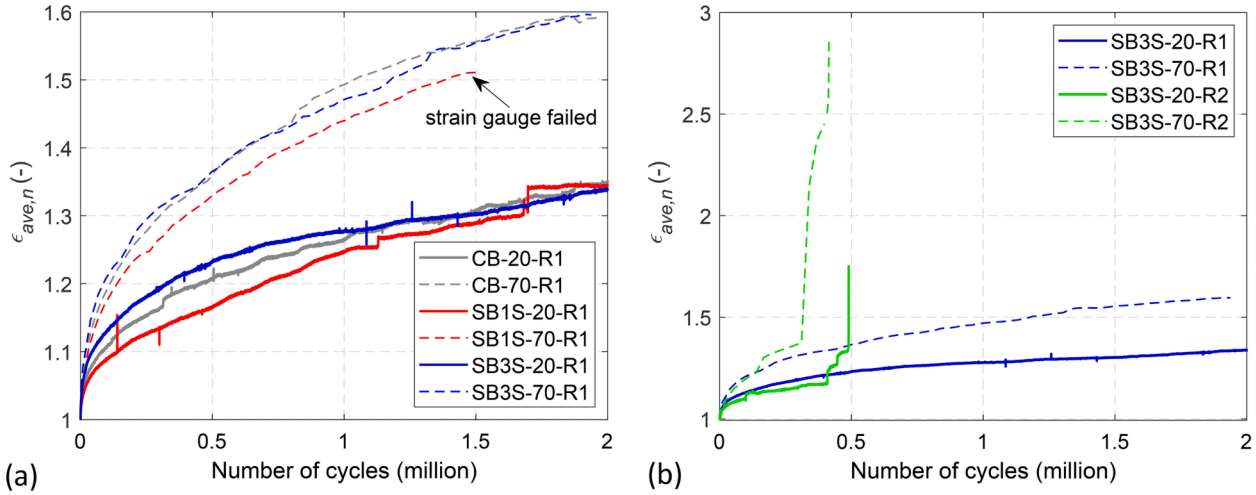

Fig. 16. Evolution of average normalized concrete strain ($\varepsilon_{ave,n}$). (a) Effect of strengthening ratio and temperature and (b) Effect of R ratio and temperature in beams with same NSM CFRP-strengthening ratio.

3.2.5. *Accumulated dissipated energy*

One of the most important aspects of structural performance under fatigue loading is the ability of a member to adequately dissipate energy [51]. Dissipated energy (E_{diss}) within a fatigue cycle is calculated as the area of the hysteric load–deflection curve at that cycle. Therefore, the accumulation/addition of the individual dissipated energies of each cycle will result in the total dissipated energy in the fatigue test. The evolution of accumulated dissipated energy ($E_{acc,diss}$) along the fatigue loading is shown in Fig. 17, in order to evaluate the effect of strengthening ratio, temperature and fatigue load level. Furthermore, the total accumulated dissipated energy at the end of fatigue test ($E_{tot,acc,diss}$) is reported in Table 6. According to experimental results, an increase in the CFRP strengthening ratio derived in larger total accumulated dissipated energy, as expected. In this regard, taking results for specimen CB-20-R1 as the reference value, the $E_{tot,acc,diss}$ was increased by 39 % and 99 % for SB1S-20-R1 and SB3S-20-R1, respectively. Similarly, the application of a high service temperature (i.e. 70 °C) and larger amplitudes in the fatigue loading (i.e. lower values of R ratio) corresponded also to larger amounts of total accumulated dissipated energy. It should be mentioned that the effect of temperature was more pronounced in strengthened RC beams. This is a sign of temperature affecting the efficiency of the strengthening system.

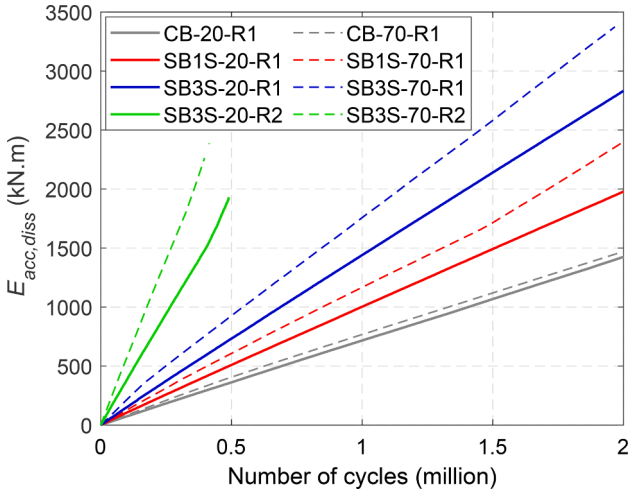

Fig. 17. Accumulated dissipated energy ($E_{acc,diss}$) versus number of cycles.

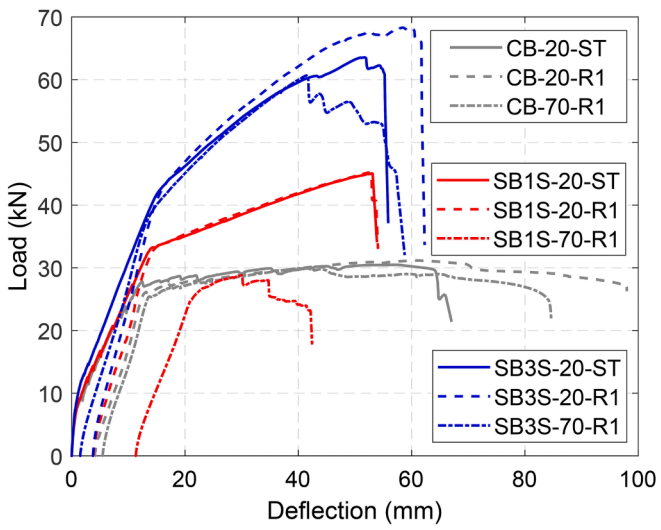

Fig. 18. Short-term and post-fatigue load–deflection curves.

3.3. *Post-fatigue residual strength*

After finishing the fatigue loading, the surviving specimens from Series 2 were unloaded and then tested up to failure in order to evaluate their residual strength. A comparison of load–deflection responses of specimens from Series 1 and 2 is shown in Fig. 18. Furthermore, the detailed results are shown in Table 7, where P_{cr} and δ_{cr} are the cracking load and the corresponding deflection; P_y and δ_y are the yielding load and the corresponding deflection; P_u and δ_u are the ultimate load and the corresponding deflection and δ_p is the plastic deflection, which was registered immediately after the unloading process of the fatigue test.

The value of δ_p defines the origin of the post-fatigue load–deflection response and it has been measured after unloading the beams (residual plastic deflection after the fatigue cycles). According to experimental results, plastic deflections, δ_p, generally increased when the temperature changed from 20 °C to 70 °C. It should be mentioned that the largest value of δ_p was registered in specimen SB1S-70-R1 ($\delta_p = 11.3$ mm) as a result of steel having worked at high levels of strains during the fatigue cycles, as explained in previous sections. The residual flexural strength depended on the level of accumulated fatigue damage in the beams. In this sense, similar values of P_y were found for short-term specimens (Series 1) and corresponding specimens in Series 2 under 20 °C. This is a sign of low damage in steel due to fatigue loading. On the contrary, larger differences between P_y in short-term specimens (Series 1) and specimens in Series 2 under 70 °C depict that steel reinforcement was damaged at the end of fatigue tests (i.e. at the beginning of post-fatigue tests). The largest reduction in P_y was observed in specimen SB1S-70-R1, and read 25 %. This is in accordance with the largest deflection and reduction in stiffness due to fatigue testing experienced by this same specimen (see Fig. 12a and 15a). An additional evidence of the damage accumulated in the steel reinforcement of specimen SB1S-70-R1 can be found in the value of P_u, which was much lower than P_y of the reference short-term specimen in Series 1 (SB1S-20-ST). To conclude, fatigue loading under large R ratio (R1) and 20 °C did not have significant effect on the residual strength of the specimens. However, the residual strength was affected by the application of 70 °C during the fatigue tests.

Table 7
Short-term and post-fatigue test results.

Specimen ID	Fatigue life (cycles)	Load (kN)			Deflections (mm)				Failure mode [b]
		P_{cr}	P_y	P_u	δ_{cr}	δ_y	δ_u	δ_p	
CB-20-ST	–	7.4	27.7	30.5	1.0	12.5	56.8	–	CC
CB-20-R1	>2,000,000	7.4[a]	26.1	31.1	1.2[a]	13.2	61.0	4.2	CC
CB-70-R1	>2,000,000	5.7[a]	25.4	30.0	1.0[a]	13.9	41.4	5.4	CC
SB1S-20-ST	–	7.4	33.1	45.0	0.9	14.6	53.0	–	FR
SB1S-20-R1	>2,000,000	7.8[a]	33.1	45.1	0.7[a]	14.7	52.4	3.8	FR
SB1S-70-R1	>2,000,000	5.9[a]	25.0	28.8	0.8[a]	21.2	30.0	11.3	SR
SB3S-20-ST	–	8.6	41.9	63.5	0.8	15.1	51.7	–	ICCS
SB3S-20-R1	>2,000,000	8.6[a]	42.4	68.3	0.7[a]	15.9	58.4	3.8	ICCS
SB3S-70-R1	>2,000,000	6.2[a]	38.3	60.6	0.8[a]	13.8	41.4	1.5	CC
SB3S-20-R2	492,600	9.1[a]	–	–	0.8[a]	–	–	–	SR
SB3S-70-R2	417,720	6.6[a]	–	–	0.8[a]	–	–	–	SR

[a] P_{cr} and δ_{cr} were calculated based on initial branch of the load–deflection curve prior to fatigue loading in Fig. 7a-10a.
[b] CC = concrete crushing; FR = FRP rupture; SR = steel reinforcement rupture; ICCS = intermediate concrete cover separation.

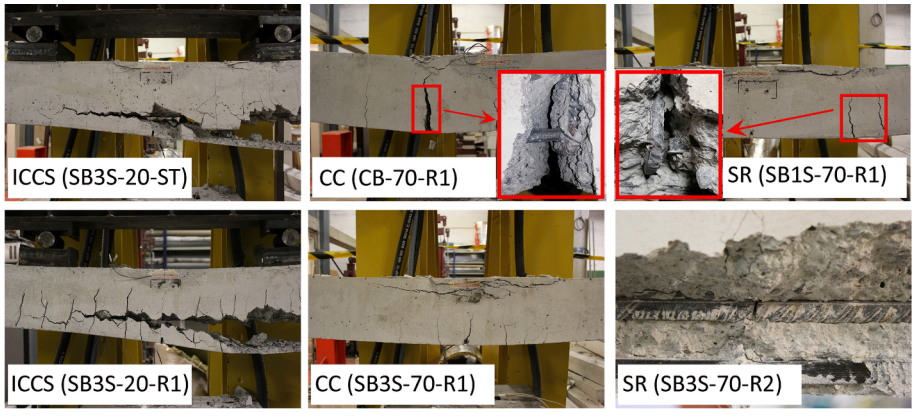

Fig. 19. Representative failure modes of the tested specimens.

3.4. Failure modes

Failure modes of specimens in Series 1 (short-term loading) and Series 2 (instantaneous post-fatigue loading in those specimens that survived fatigue loading) are detailed in Table 7, and representative images are shown in Fig. 19. According to experimental results, failure mode for unstrengthened beams did not change due to the application of a fatigue loading; therefore, the unstrengthened beams in Series 1 and 2 failed by concrete crushing (CC) after steel yielding. It should be mentioned, however, that a large strain was observed in specimens CB-20-R1 and CB-70-R1 (see zoom view regarding to specimen CB-70-R1 in Fig. 19). Regarding the specimens strengthened with one CFRP strip, experimental results confirm that fatigue loading at 20 °C did not cause significant damage, so that specimens SB1S-20-ST and SB1S-20-R1 experienced same failure mode, i.e. FRP rupture (FR). Similar behavior was observed in [37]. However, the application of a higher temperature during the fatigue tests caused a change in failure mode, and specimen SB1S-70-R1 failed by steel reinforcement rupture (SR). This is an evidence of a highly demanded steel reinforcement, due to bond deterioration, during fatigue loading. This bond deterioration in the beam was also clear from load-deflection response in Fig. 18, where the ultimate load of this strengthened beam was smaller than corresponding unstrengthened control beam. Finally, the negligible damage caused in steel due to fatigue loading under 20 °C was also confirmed in failure modes of specimens strengthened with three strips, so that specimens SB3S-20-ST and SB3S-20-R1 failed by intermediate concrete cover separation (ICCS), which was due to unstable diagonal crack that propagated along the height of the section. It should be mentioned that specimens subjected to a lower R ratio (R2) did not survive the programmed fatigue test (i.e. failed by SR during the fatigue loading) and, therefore, they cannot be included in the analysis of the post-fatigue failure mode. However, for illustrative purposes, a representative image has been included in Fig. 19.

4. Conclusions

The present experimental work aimed to study the effect of fatigue loading on the flexural performance of NSM CFRP-strengthened RC beams under two different service temperatures. An experimental campaign consisting of 11 specimens (3 beams tested under short-term loading as reference specimens and 8 beams tested under fatigue loading) was performed, where beams with different amounts of CFRP strengthening ratio, different fatigue load level and different temperature were loaded for 2 million cycles or failure, whichever happens first, at a frequency of 2 Hz. After that, post fatigue tests were carried out to analyze the residual flexural strength.

As a general conclusion, the increase in the testing temperature resulted in a decrease in the stiffness and the residual strength. Besides, due to bigger hysteric loops, specimens under 70 °C showed a larger amount of accumulated dissipated energy. Based on the test configuration and setup adopted, the NSM strengthening system showed a good fatigue flexural performance when subjected to testing temperature beyond the T_g of the epoxy adhesive.

A list of detailed conclusions from the experimental tests is presented next:

- Specimens tested under a large R ratio (R1 = 0.57) could withstand the whole fatigue test (i.e. 2 million cycles), whilst rupture of steel reinforcement during fatigue loading took place for low R ratios (R2 = 0.38).
- As the fatigue test progressed, the deflection and concrete strain increased and the stiffness decreased, with the larger rates of variation corresponding to the initial stages of cyclic loading. Besides, in general, the NSM CFRP-strengthened RC beams showed a better fatigue performance when compared to unstrengthened control beams.
- The effect of temperature was more pronounced when combined with low R ratio. Therefore, the combined effect of both parameters should be considered in evaluating the fatigue life of the members.
- NSM CFRP-strengthening helped to postpone the failure of the beam during fatigue loading after steel reinforcement rupture. In this sense, fatigue life was extended in about 22 %.
- Larger CFRP strengthening ratios and higher testing temperature resulted in larger dissipated energy, whereas R ratio had the opposite effect.
- The residual strength of the specimens depended on the level of fatigue damage. In this sense, residual strength decreased for NSM CFRP-strengthened specimens under 70 °C, especially for the strengthened beam with low CFRP ratio.
- Fatigue testing did not affect post-fatigue failure mode of unstrengthened beams. For the case of strengthened beams under R1, the application of 70 °C during the fatigue loading caused the change in post-fatigue failure mode.

Declaration of Competing Interest

The authors declare that they have no known competing financial interests or personal relationships that could have appeared to influence the work reported in this paper.

Data availability

Data will be made available on request.

Acknowledgements

This research was supported by the Spanish Ministry of Science and Innovation (MCIN/ AEI) under project PID2020-119015GB-C22, the Generalitat de Catalunya under the grant number 2019FI_B 00054 and mobility grant from Universitat de Girona (MOB 2021). The authors also wish to acknowledge the support of S&P Clever Reinforcement Ibérica Lda. for supplying the epoxy resin and the CFRP laminate used in this study.

References

[1] Kim YJ, Heffernan PJ. Fatigue behavior of externally strengthened concrete beams with fiber-reinforced polymers: State of the art. J Compos Constr 2008;12(3):246–56. https://doi.org/10.1061/(ASCE)1090-0268(2008)12:3(246).
[2] Oudah F, El-Hacha R. Research progress on the fatigue performance of RC beams strengthened in flexure using Fiber Reinforced Polymers. Compos Part B 2013;47:82–95. https://doi.org/10.1016/j.compositesb.2012.09.057.
[3] Zhu Z, Zhu E, Ni Y, Li D. Flexural fatigue behavior of large-scale beams strengthened with side near surface mounted (SNSM) CFRP strips. Eng Struct 2019;180:134–47. https://doi.org/10.1016/j.engstruct.2018.11.039.
[4] Dineshkumar R, Ramkumar S. Review paper on fatigue behavior of reinforced concrete beams. Mater Today: Proc 2020;21:19–23. https://doi.org/10.1016/j.matpr.2019.05.353.
[5] Chen C, Cheng L. Fatigue life-based design of RC beams strengthened with NSM FRP. Eng Struct 2017;140:256–66. https://doi.org/10.1016/j.engstruct.2017.02.065.
[6] Siddika A, Al Mamun MA, Alyousef R, Amran YM. Strengthening of reinforced concrete beams by using fiber-reinforced polymer composites: A review. J Build Eng 2019;25:100798. https://doi.org/10.1016/j.jobe.2019.100798.
[7] Pellegrino C, Sena-Cruz J. Design Procedures for the Use of Composites in Strengthening of Reinforced Concrete Structures. State-of-the-Art Report of the Rilem Technical Committee. Springer, The Netherlands, 2016. https://doi.org/10.1007/978-94-017-7336-2.
[8] De Lorenzis L, Teng JG. Near-surface mounted FRP reinforcement: An emerging technique for strengthening structures. Compos Part B 2007;38(2):119–43. https://doi.org/10.1016/j.compositesb.2006.08.003.
[9] Jahani Y, Baena M, Barris C, Perera R, Torres L. Influence of curing, post-curing and testing temperatures on mechanical properties of a structural adhesive. Constr Build Mater 2022;324:126698. https://doi.org/10.1016/j.conbuildmat.2022.126698.
[10] Silva P, Fernandes P, Sena-Cruz J, Xavier J, Castro F, Soares D, et al. Effects of different environmental conditions on the mechanical characteristics of a structural epoxy. Compos Part B 2016;88:55–63. https://doi.org/10.1016/j.compositesb.2015.10.036.

[11] Firmo JP, Roquette MG, Correia JR, Azevedo AS. Influence of elevated temperatures on epoxy adhesive used in CFRP strengthening systems for civil engineering applications. Int J Adhes Adhes 2019;93:102333. https://doi.org/10.1016/j.ijadhadh.2019.01.027.
[12] Michel M, Ferrier E. Effect of curing temperature conditions on glass transition temperature values of epoxy polymer used for wet lay-up applications. Constr Build Mater 2020;231:117206. https://doi.org/10.1016/j.conbuildmat.2019.117206.
[13] Al-Abdwais AH, Al-Mahaidi RS. Experimental and finite element analysis of flexural performance of RC beams retrofitted using near-surface mounted with CFRP composites and cement adhesive. Eng Struct 2021;241:112429. https://doi.org/10.1016/j.engstruct.2021.112429.
[14] Barris B, Sala P, Gómez J, Torres L. Flexural behaviour of FRP reinforced concrete beams strengthened with NSM CFRP strips. Compos Struct 2020;241:112059. https://doi.org/10.1016/j.compstruct.2020.112059.
[15] Dias SJ, Barros JA, Janwaen W. Behavior of RC beams flexurally strengthened with NSM CFRP laminates. Compos Struct 2018;201:363–76. https://doi.org/10.1016/j.compstruct.2018.05.126.
[16] El-Hacha R, Rizkalla SH. Near-surface-mounted fiber-reinforced polymer reinforcements for flexural strengthening of concrete structures. ACI Struct J 2004;101:717–26. https://doi.org/10.14359/13394.
[17] Parretti R, Nanni A. Strengthening of RC members using near-surface mounted FRP composites: Design overview. Adv Struct Eng 2004;7(6):469–83. https://doi.org/10.1260/1369433042863198.
[18] Jahani Y, Baena M, Gómez J, Barris C, Torres L. Experimental Study of the Effect of High Service Temperature on the Flexural Performance of Near-Surface Mounted (NSM) Carbon Fiber-Reinforced Polymer (CFRP)-Strengthened Concrete Beams. Polymers 2021;13(6):920. https://doi.org/10.3390/polym13060920.
[19] Silva P, Escusa GG, Sena-Cruz J, Azenha M. Experimental investigation of RC slabs strengthened with NSM CFRP system subjected to elevated temperatures up to 80 °C. In Proc. 8th Int. Conf. on Fibre-Reinforced Polymer (FRP) Composites in Civil Engineering, CICE, Hong Kong, China, 2016. http://hdl.handle.net/1822/43902.
[20] Azevedo AS, Firmo JP, Correia JR, Tiago C. Influence of elevated temperatures on the bond behaviour between concrete and NSM-CFRP strips. Cem Concr Compos 2020;111:103603. https://doi.org/10.1016/j.cemconcomp.2020.103603.
[21] Aidoo J, Harries KA, Petrou MF. Fatigue behavior of carbon fiber reinforced polymer-strengthened reinforced concrete bridge girders. J Compos Constr 2004;8(6):501–9. https://doi.org/10.1061/(ASCE)1090-0268(2004)8:6(501).
[22] Barnes RA, Mays GC. Fatigue performance of concrete beams strengthened with CFRP plates. J Compos Constr 1999;2:63–72. https://doi.org/10.1061/(ASCE)1090-0268(1999)3:2(63).
[23] Heffernan PJ, Erki MA. Fatigue behavior of reinforced concrete beams strengthened with carbon fiber reinforced plastic laminates. J Compos Constr 2004;8(2):132–40. https://doi.org/10.1061/(ASCE)1090-0268(2004)8:2(132).
[24] Ekenel M, Rizzo A, Myers JJ, Nanni A. Flexural fatigue behavior of reinforced concrete beams strengthened with FRP fabric and precured laminate systems. J Compos Constr 2006;10(5):433–42. https://doi.org/10.1061/(ASCE)1090-0268(2006)10:5(433).
[25] Dong Y, Ansari F, Karbhari VM. Fatigue performance of reinforced concrete beams with externally bonded CFRP reinforcement. Struct Infrastruct Eng 2011;7(3):229–41. https://doi.org/10.1080/15732470802383669.
[26] Toutanji H, Zhao L, Deng Y, Zhang Y, Balaguru P. Cyclic behavior of RC beams strengthened with carbon fiber sheets bonded by inorganic matrix. J Mater Civ Eng 2006;18(1):28–35. https://doi.org/10.1061/(ASCE)0899-1561(2006)18:1(28).
[27] Lin JX, Huang PY, Guo YC, Guo XY, Zeng JJ, Zhao C, et al. Fatigue behavior of RC beams strengthened with CFRP laminate under hot-wet environments and vehicle random loads coupling. Int J Fatigue 2020;131:105329. https://doi.org/10.1016/j.ijfatigue.2019.105329.
[28] Song L, Yu Z. Fatigue performance of corroded reinforced concrete beams strengthened with CFRP sheets. Constr Build Mater 2015;90:99–109. https://doi.org/10.1016/j.conbuildmat.2015.05.024.
[29] Gallego JM, Czaderski C, Breveglieri M, Michels J. Fatigue behaviour at elevated temperature of RC slabs strengthened with EB CFRP strips. Compos Part B 2018;141:37–49. https://doi.org/10.1016/j.compositesb.2017.12.026.
[30] Badawi M, Soudki K. Fatigue behavior of RC beams strengthened with NSM CFRP rods. J Compos Constr 2009;13(5):415–21. https://doi.org/10.1061/(ASCE)1090-0268(2009)13:5(415).
[31] Wahab N, Soudki KA, Topper T. Mechanics of bond fatigue behavior of concrete beams strengthened with NSM CFRP rods. J Compos Constr 2011;15(6):934–42. https://doi.org/10.1061/(ASCE)CC.1943-5614.0000228.
[32] Chen C, Cheng L. Fatigue behavior and prediction of NSM CFRP-strengthened reinforced concrete beams. J Compos Constr 2016;20(5):04016033. https://doi.org/10.1061/(ASCE)CC.1943-5614.0000691.
[33] Al-Saadi NTK, Mohammed A, Al-Mahaidi R. Fatigue performance of near-surface mounted CFRP strips embedded in concrete girders using cementitious adhesive made with graphene oxide. Constr Build Mater 2017;148:632–47. https://doi.org/10.1016/j.conbuildmat.2017.05.103.
[34] Fernandes PM, Silva PM, Sena-Cruz J. Bond and flexural behavior of concrete elements strengthened with NSM CFRP laminate strips under fatigue loading. Eng Struct 2018;84:350–61. https://doi.org/10.1016/j.engstruct.2014.11.039.
[35] Charalambidi BG, Rousakis TC, Karabinis AI. Fatigue behavior of large-scale reinforced concrete beams strengthened in flexure with fiber-reinforced polymer laminates. J Compos Constr 2016;20(5):04016035. https://doi.org/10.1061/(ASCE)CC.1943-5614.0000689.
[36] Quattlebaum JB, Harries KA, Petrou MF. Comparison of three flexural retrofit systems under monotonic and fatigue loads. J Bridge Eng 2005;10(6):731–40. https://doi.org/10.1061/(ASCE)1084-0702(2005)10:6(731).
[37] Sena-Cruz J, Barros JA, Coelho MR, Silva LF. Efficiency of different techniques in flexural strengthening of RC beams under monotonic and fatigue loading. Constr Build Mater 2012;29:175–82. https://doi.org/10.1016/j.conbuildmat.2011.10.044.
[38] UNE-EN 12390-3. Testing Hardened Concrete—Part 3: Compressive Strength of Test Specimens; AENOR: Madrid, Spain, 2003.
[39] UNE-EN 12390-6. Testing Hardened Concrete—Part 6: Tensile Splitting Strength of Test Specimens; AENOR: Madrid, Spain, 2010.
[40] ASTM C469/C469M-14. Standard Test Method for Static Modulus of Elasticity and Poisson's Ratio of Concrete in Compression; ASTM International: West Conshohocken, PA, USA, 2014.
[41] UNE-EN ISO 15630-1. Steel for the Reinforcement and Prestressing of Concrete-Test Methods—Part 1: Reinforcing Bars, Wire Rod and Wire; AENOR: Madrid, Spain, 2011.
[42] S&P. S&P Cfrp Laminate, Technical Datasheet; S&P: Seewen, Switzerland, 2017.
[43] ISO 527-5. Plastics-Determination of Tensile Properties—Part 5: Test Conditions FOR Unidirectional Fibre-Reinforced Plastic Composites; ISO: Geneva, Switzerland, 2009.
[44] S&P. S&P Resin 220 HP Epoxy Adhesive, Technical Data Sheet; S&P: Seewen, Switzerland, 2019.
[45] ASTM E1356-08. Standard Test Method for Assignment of the Glass Transition Temperatures by Differential Scanning Calorimetry; ASTM International: West Conshohocken, PA, USA, 2008.
[46] ASTM D5023-15. Standard Test Method for Plastics: Dynamic Mechanical Properties: In Flexure (Three-Point Bending); ASTM International: West Conshohocken, PA, USA, 2015.
[47] ISO 527-1. Plastics-Determination of Tensile Properties—Part 1: General Principles; ISO: Geneva, Switzerland, 2012.
[48] ACI 440.2R-17. Guide for the Design and Construction of Externally Bonded FRP Systems for Strengthened Concrete Structure. American concrete Institute, ACI, Farmington Hills, MI, USA, 2017.
[49] Fib Bulletin 90. Externally Applied FRP Reinforcement for Concrete Structures; International Federation for Structural Concrete: Lausanne, Switzerland, 2019.
[50] Breveglieri M, Czaderski C. RC slabs strengthened with externally bonded CFRP strips under long-term environmental exposure and sustained loading. Part 2: Laboratory experiments. JCOMC 2021;6:100210. https://doi.org/10.1016/j.jcomc.2021.100210.
[51] Darwin David, Nmai Charles K. Energy Dissipation in RC Beams Under Cyclic Load. J Struct Eng 1986;112(8):1829–46. https://doi.org/10.1061/(ASCE)0733-9445(1986)112:8(1829).